Crack Initiation and Propagation on AISI-SAE Stainless Steel 304 Under Rotating Bending Fatigue Tests and Close to Elastic Limit

G.M. Domínguez Almaraz[1]. V.H. Mercado Lemus[1], M.L. Mondragón Sánchez[2]

[1] Universidad Michoacana de San Nicolás de Hidalgo, Facultad de Ingeniería Mecánica, Santiago Tapia No. 403, Col. Centro, 58000, Morelia Mich., dalmaraz@umich.mx.
[2] Instituto Tecnológico de Morelia, Postgrado en Metalurgia, Av. Tecnológico 1500, Colonia Lomas de Santiaguito, C.P. 58120, Morelia, Mich., México.

ABSTRACT. *This work deals with crack initiation and propagation on AISI 304 stainless steel undergoing rotating bending fatigue tests and loading stresses close the elastic limit of material. Simulation results are obtained by Visual Nastran software in order to determine the numerical stresses and strains distributions inside the specimen; then, this information is used for the experimental set up. A general description concerning the experimental test machine and experimental conditions are developed in further sections. Later, experimental results are presented and discussed according the observed crack origin related to high stress zones. Finally, a simple model is proposed involving the plastic strain at fracture, the crack propagation and the total fatigue life for this steel loaded close to its elastic limit.*

INTRODUCTION

Stainless steels have been manufactured and used from the beginning of last century; nevertheless, the improvements on physical and mechanical properties in last decades allow diversifying the industrial application of these alloys. Austenitic stainless steels present no magnetic properties and are commonly used in food, health, transport, energy production and heat exchange, chemical, electronic and nuclear industries. The nomination AISI 304 is known as the "all applications stainless steel" due to its wide range of industrial use. Resent work on fatigue endurance and crack initiation and propagation on stainless steels has been carried out coupling simulation results by Finite Element Method with a multiaxial fatigue criterion for the crack initiation and growth prediction, together with experimental results [1]. This approach applies for the prediction of fatigue behavior of notched members under constant-amplitude loading and step loading. Nevertheless, assuming that real material is a Continuous Medium and that stress and strain distributions obtained by numerical simulation represent real conditions may lead to miscalculations. Furthermore, fatigue failure on stainless steels is often related to stress concentration developed close to impurities and discontinuities inside the material [2], and these ones are not generally included in numerical

simulations. Furthermore, the separation point between crack initiation and propagation is not still clear after a large number of studies in steels; recent works [3, 4] accord that most of fatigue life (above 90%) is consumed in crack initiation and that the corresponding physical mechanisms are developed at crystallographic scale [5]. A dual scale approach [6], has been developed in an attempt to understand the physical behavior of crack initiation and propagation at micro and macro material scale; however, few studies have been oriented to investigate the crack initiation and propagation on stainless steels under high cycling loading (high plastic deformation). A new high speed (150 Hz) rotating bending fatigue test machine [7] has been build up to perform the results herein presented.

Testing Material

AISI 304 stainless steel is a well weldable and high temperature resistance material with low carbon content. Table 1 presents the corresponding chemical composition and Table 2 the mechanical properties.

Table 1. Chemical composition (% weight)

C	Cr	Ni	Mn	Si	P	S
0.08 max	18 - 20	8 - 11	2 max	1 max	0.04 max	0.03 max

Table 2. Mechanical properties

Density (Kg/m^3)	E (Gpa)	Yield stress (MPa)	Ultim. stress (MPa)	Hardness (HRB)
7900	193	760	1100	97

Testing machine

Figure 1 shows the principal components of the high speed rotating bending machine: electrical motor **1** provides motion to rotating axis **2** which is connected to specimen **3**. Electronic system (not shown) located close to back side of rotating axis is destined to count the number of cycles; it is composed by an electronic sensor, electronic card, personal computer and software. The applying load system **4** is simplified in Figure 1; it consists of a bearing at the free side of specimen allowing communicating the applied load P and a spring frame supporting the bearing. When the specimen is failing the distance between this one and the proximity sensor **5** increases, this leads to the automatic stop of electrical motor and test by electric relay **6**.

Specimen

Tests were carried out on hourglass shape specimens with the dimensions shown in Figure 2. No international standardization is available for the rotating bending fatigue

specimens; thus, narrow section diameter D_0 was determined by numerical simulation varying the applied load P for the corresponding mechanical properties of this steel, in order to induce stresses in the narrow section close to elastic limit (75%), Figure 3. During the test, temperature at the specimen narrow section is controlled by a cooling system with pressurized cool air.

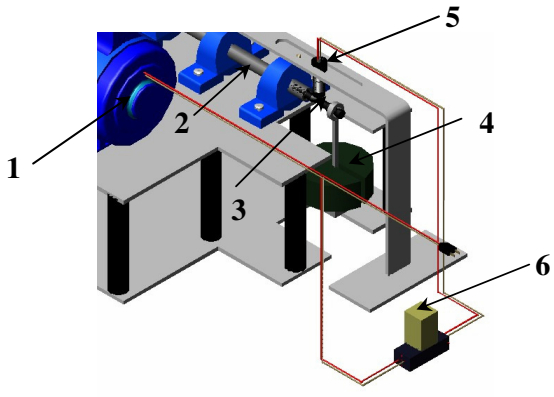

Figure 1. Principal components of high speed rotating bending machine.

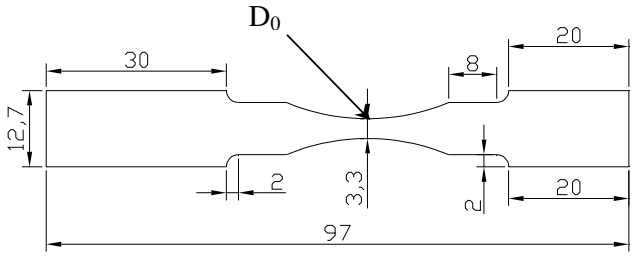

Figure 2. Dimensions (mm) of testing specimen.

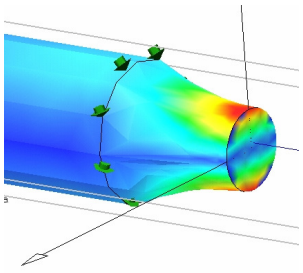

Figure 3. Numerical results for rotating bending fatigue specimen.

RESULTS

Table 1 presents the tests parameters and fatigue endurance results on this stainless steel when the applying load P induces stresses close to 75% of the elastic limit of material.

Table 3. Testing parameters and fatigue endurance results on AISI 304 stainless steel.

Test No.	D_0 (mm)	P (N)	Number of Cycles	Temperature (ºC)
1	3.3	40	22350	35
2	3.3	40	18800	32
3	3.3	40	15300	30
4	3.3	40	28875	34
5	3.3	40	17450	33
6	3.3	40	33550	32
7	3.3	40	36560	31
8	3.3	40	40250	35
9	3.3	40	40010	32
10	3.3	40	25600	30
11	3.3	40	32550	35
12	3.3	40	23450	33

Temperature was measured at fracture surface after specimen cracking, last column. Figure 4 shows the fracture surface of specimen number 9 listed on Table 3. Fatigue crack initiation in metals generally presents a slowly grow on a perpendicular plane with regard to applied load; this plane direction is modified with crack grow until an angle of 45º is reached. The final rotation angle on crack propagation occurs at the transition point where the onset of fast crack propagation takes place [8]. In Figure 4 are shown different crack initiation points around the perimeter of fracture surface, where highest stress zones are located under rotating bending fatigue.

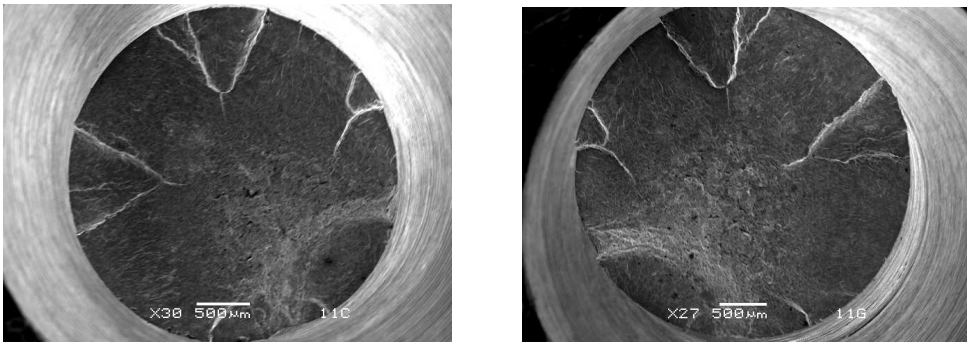

a) b)

Figure 4. Fracture surfaces: a) right and b) lefth on specimen No.9

Three transitions points are clearly observed in Figure 4; the origins are located at the specimen surface (perimeter on fracture surface) and present a convergence triangular tendency towards the center of fracture surface. The triangle vertexes close to fracture surface center are the transitions points.

DISCUSSION

Fatigue endurance in ductile materials is related to plastic deformation inside the material: partial mechanical energy from applied load is transformed to plastic deformation energy [9]. In this process the mechanical properties decrease gradually whit the increase of plasticity; particularly, the remaining ductility and the elastic stiffness. Recent works [10, 11], have postulated the "Damage rule" to approach a realistic evolution law and the consequences of damage to material strength: ductility damage is defined as the relative reduction of deformability to quantify damage. The power law damage evolution is:

$$dD = m\left[\frac{\varepsilon_p}{\varepsilon_f}\right]^{m-1}\frac{d\varepsilon_p}{\varepsilon_f} \tag{1}$$

Where: dD is the differential variation on ductility damage, m is the damage exponent for the evolution law, ε_p is the current plastic strain and ε_f is the strain in the fracture envelope located at the "Cylindrical decomposition of damage" [11]. Integration on dD yields:

$$D = \int_0^{\varepsilon c} dD = 1 \tag{2}$$

In last expression, ε_c is the plastic strain at fracture on the given loading history and $\varepsilon_c = \varepsilon_f$ for a single value of m and ε_f = constant. The strain ε_f is expressed by:

$$\varepsilon_f = \varepsilon_{f0}\mu_p(p)\mu_\chi(\chi) \tag{3}$$

Here, ε_{f0} is a reference fracture strain indicated by zero mean stress tension and the functions $\mu_p(p)$ and $\mu_\chi(\chi)$ represent the pressure and Lode angle dependence, respectively. Plastic strain ε_p is generally no constant along the deformation path; then, this variable strain should be associated with each step of loading by the equation:

$$\varepsilon_p = c\frac{\varepsilon_{f0}}{N^k} \tag{4}$$

Reprenting the current plastic strain at each loading step N, with: $k \neq m$ and c = constant. The value of ε_p is higher in the first steps and decreases to cero at fracture (at total number of cycles N_f). Integrating and solving last equation gives:

$$\varepsilon_c = \int_1^{Nf} \varepsilon_p = c\varepsilon_{f0} \int_1^{Nf} \frac{1}{N^k} dN = \frac{c\varepsilon_{f0}}{-k+1} N^{-k+1} \Big|_1^{Nf} \tag{5}$$

The plastic strain at fracture ε_c is a function of the material isotropic property ε_{fo}, the constant k which is related to ductility, the constant c which is a function of hardness and loading conditions and the total fatigue cycles N_f to fracture. If k and c increase (ductile material and high loading regime), $d\varepsilon_p/dN$ is higher in the first N fatigue steps; furthermore, ε_c increases even if N_f decreases because the high loading regime. Figure 5 presents the graph ε_p – N; the total area below the curve is ε_c and the tangent at each point is $d\varepsilon_p /dN$.
Taking the specimen No. 9 in Table 3, the values are: N_f = 40,000 cyles, k = 0.5 ($0 < k < 1$), ε_{fo} = 0.8 and c = 4 x 10^{-3}, that yields: ε_c = 1.27 (curve in red).

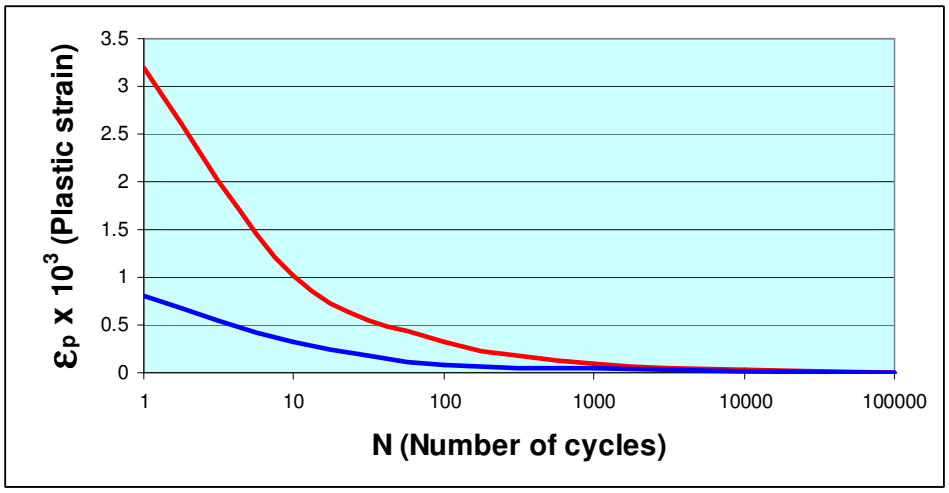

Figure 5. Evolution of ε_p with the number of cycles for two materials.

The curve in blue has been estimated for a different material: c = 0.001, k = 0.4, N_f = 70000 cycles and the same loading regime (75% of elastic limit). Increase in hardness lead to decrease c and k; then, plastic strain at fracture in this case is lower than the previous one: ε_c = 1.07 (curve in blue) as it is shown in Figure 5 by the areas below the corresponding curves, even if N_f increases for the blue line.

CONCLUSION

Fatigue loading on metallic alloys systematically leads to plastic strain at micro or micro-macro scales [12, 13, 14]. Furthermore, crack initiation and propagations is closely related to plasticity development on one site (or different sites) inside the material; then, the plasticity initiation and propagation should be coupled to crack initiation and propagation [15, 16, 17]. In this work is presented a simple model associating the plastic strain at fracture with: the number of cycles of fatigue life, the isotropic properties of material and two constant related to hardness and loading regime. Current plastic strain is higher in the first fatigue steps and decreases with the number of cycles until fracture. Plastic strain at fracture is higher for ductile alloys undergoing high loading, even if fatigue life decreases. No intermediate effects such as hardening rule (change in yield condition with the progression of plastic deformation) were taken into account in this model.

ACKNOWLEDGEMENTS

We want to express our gratitude to the University of Michoacan (UMSNH) and the Technologic Institute of Morelia (ITM) in Mexico for the facilities received to carry out this work; a special mention of gratitude to CONACYT (The National Counsel for Science and Technology in Mexico) for the financial support destined to this project.

REFERENCES

1. Feifei F., Kalnaus S., Yanyao J. (2008) *J. Mech. Of Mate.*, **40**, 961-973.
2. Masaki K., Ochi Y., Matsumura T., (2006) *Int. Jour. Fatig*., **28**, 1603-1610.
3. Bathias C., Paris P.C. (2005) *Gigacycle fatigue in mechanical practice*, Marcel Dekker (Ed.) New York.
4. Ravichandran K.S., Ritchie R.O., Murakami Y., (1999) *Small fatigue cracks: mechanics, mechanisms and applications*, Elsevier, New York.
5. Paris P.C., Lados D., Tada H., (2008), *Eng. Fract. Mecha.,* **75***,* 299-305.
6. Sih G.C. (2008) *Theoret. and Appl. Fract. Mech.*, **50**, 142-156.
7. Dominguez almaraz G., Guzmán Tapia M., (2007) *Fourth International Conference on Very High Cycle Fatigue (VHCF-4), Ann Arbor, University of Michigan, August 19-22,* 153-160.
8. Sih G.C. (1988) *Theoret. and Appl. Fract. Mech.*, **9**, 175-198.
9. Lemaître J. A. (1985) *J. Engng. Mater. Technol.* – Trans ASME, **107**, 83–90.
10. Xue L. (2007) Int. J. Solids Struct. **44**, 5163–81.
11. Xue L., Wierzbicki T. (2008) *J. Engng Fract. Mech.*, **75**, 3276-93.
12. Ladani L., Dasgupta A. (2008) *Int. Jour. Fatig.*, article in press.
13. Stouffer CD, Dame LT.(1996) *Inelastic deformation of metals: models, mechanical properties, and metallurgy*. New York, US: John Wiley & Sons Inc.

14. Lämmer H, Tsakmakis CH. (2000) *Int. J. Plasticity*, **16**(5), 495–523.
15. Sackett E.E, Germain L., Bache M.R. (2007) *Int. Jour. Fatig.*, **29**(9-11), 2015-2021.
16. Hirakata H., Takahashi Y.,Truong D.V., Kitamura T. (2007) *Int. Jour. Fract.*, **145** (4), 261-271.
17. Lukas P., Kunz L. (2002) *Mat. Scie., and Engin. A*, **322**(1), 217-227.